Molecular Therapy
Methods & Clinical Development
Original Article

Temporal insights into molecular and cellular responses during rAAV production in HEK293T cells

Alok Tanala Patra,[1] Evan Tan,[1] Yee Jiun Kok,[1] Say Kong Ng,[1] and Xuezhi Bi[1,2,3]

[1]Bioprocessing Technology Institute (BTI), Agency for Science, Technology and Research (A*STAR), Singapore 138668, Singapore; [2]Duke-NUS Medical School, National University of Singapore, Singapore 169857, Singapore; [3]Food, Chemical and Biotechnology Cluster, Singapore Institute of Technology, Singapore 138683, Singapore

The gene therapy field seeks cost-effective, large-scale production of recombinant adeno-associated virus (rAAV) vectors for high-dosage therapeutic applications. Although strategies like suspension cell culture and transfection optimization have shown moderate success, challenges persist for large-scale applications. To unravel molecular and cellular mechanisms influencing rAAV production, we conducted an SWATH-MS proteomic analysis of HEK293T cells transfected using standard, sub-optimal, and optimal conditions. Gene Ontology and pathway analysis revealed significant protein expression variations, particularly in processes related to cellular homeostasis, metabolic regulation, vesicular transport, ribosomal biogenesis, and cellular proliferation under optimal transfection conditions. This resulted in a 50% increase in rAAV titer compared with the standard protocol. Additionally, we identified modifications in host cell proteins crucial for AAV mRNA stability and gene translation, particularly regarding AAV capsid transcripts under optimal transfection conditions. Our study identified 124 host proteins associated with AAV replication and assembly, each exhibiting distinct expression pattern throughout rAAV production stages in optimal transfection condition. This investigation sheds light on the cellular mechanisms involved in rAAV production in HEK293T cells and proposes promising avenues for further enhancing rAAV titer during production.

INTRODUCTION

Gene therapy has emerged as a promising treatment approach for a number of genetic diseases, certain cancers, and other infectious diseases. Among the several types of viral or non-viral gene delivery vectors available, recombinant adeno-associated virus (rAAV) is currently the main viral vector of choice for gene delivery to treat a variety of human genetic diseases such as hemophilia, cystic fibrosis, muscular dystrophy, and cancer.[1–4] The AAVs are non-pathogenic members of the Parvoviridae family with compact genomes that have emerged as versatile tools in diverse biomedical applications, including gene editing and vaccine development. Their unique properties, including efficient tissue-specific gene delivery with minimal off-target effects and sustained transgene expression, have driven their increasing popularity as vectors for gene therapy.[5–9] One pivotal challenge within this landscape centers on identifying optimal transfection conditions capable of augmenting the production of high-titer rAAVs containing the desired gene of interest (GOI).[10–12] Ensuring a substantial quantity of fully loaded rAAV particles carrying the GOI also remains a hurdle to surmount. The existing literature exposes a knowledge gap in the exploration of molecular and cellular dynamics related to HEK293T cells during rAAV production, notwithstanding their widespread use in the biomanufacturing industry. Previous studies have primarily focused on rAAV yield in various design of experiment (DoE) transient transfection conditions,[13–16] or concentrated solely on comparing transfected vs. untransfected HEK293 cell lines at a single harvest time point.[17,18] There are limited insights into the molecular dynamics underlying the conditions associated with higher rAAV production and the temporal changes across various cellular states during the AAV production process.

To address the knowledge gap in understanding host cell responses during rAAV production, this study employed an SWATH-mass spectrometry (MS) workflow with a custom-built HEK293T-AAV spectral library for a comprehensive temporal analysis of the cellular states under various transfection conditions associated with differential rAAV2 titer. Proteomic landscape derived from standard (unoptimized), sub-optimal and optimal transfection conditions, involving varying parameters for initial transfection cell density, total plasmid DNA concentration, and plasmid ratios, were examined at 24, 48, and 72 h post-transfection (hpt). Leveraging on the custom-built spectral library (comprising 7,183 protein groups), we successfully identified ~4,800 proteins for comparative proteomic analysis, which shed light on the dynamic interplay between HEK293T cellular states and rAAV production and provided valuable insights to refine bioprocessing strategies for future rAAV manufacturing.

Received 16 December 2023; accepted 4 June 2024;
https://doi.org/10.1016/j.omtm.2024.101278.

Correspondence: Xuezhi Bi, Bioprocessing Technology Institute (BTI), Agency for Science, Technology and Research (A*STAR), Singapore 138668, Singapore.
E-mail: bi_xuezhi@bti.a-star.edu.sg

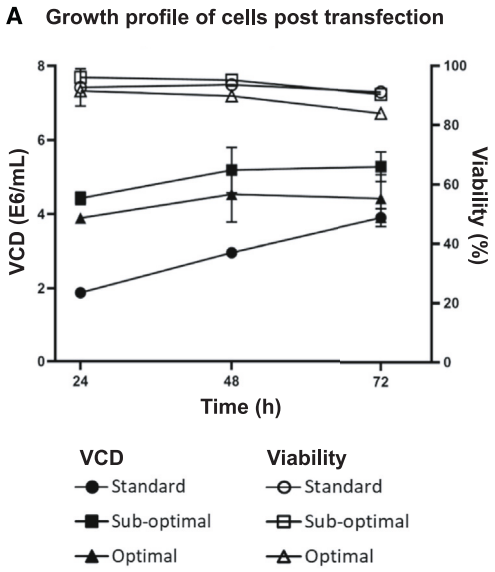

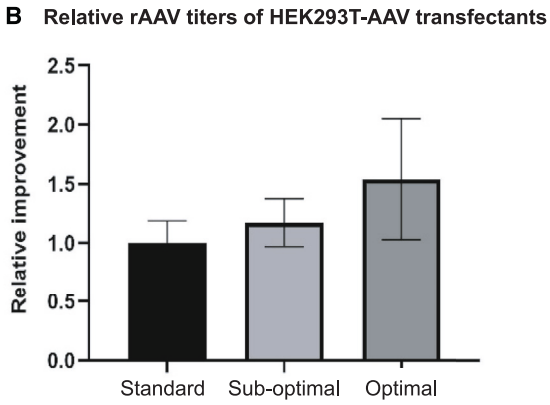

Transfectants	Titer (E14 vg/L)
Standard	2.38 ± 0.45
Sub-optimal	2.79 ± 0.48
Optimal	3.66 ± 1.22

Figure 1. Growth profiles of cells post-transfection and rAAV titers

(A) Viability and viable cell density (VCD) of cells post-transfection. (B) Cells were harvested 72 h post-transfection for rAAV titering. Optimization of transfection conditions gave an ∼50% increase in rAAV titers obtained.

RESULTS

Cell culture profiles under different transfection conditions

For standard baseline condition, transfection was conducted at a cell density of 1 × 10^6 cells/mL with defined pHelper:pAAV_RC2:pAAV_GFP ratio of 1:1:1. Sub-optimal and optimal transfections were performed at higher cell density of 2.5 × 10^6 cells/mL using proprietary plasmid ratios. Growth profile of transfected cells and corresponding rAAV titers measured from un-purified rAAV2 in cell lysates at 72 hpt are shown in Figure 1, with obtained titers of the following: standard transfection – 2.38 ± 0.45 E14 vg/L, sub-optimal transfection – 2.79 ± 0.48 E14 vg/L, and optimal transfection – 3.66 ± 1.22 E14 vg/L. Optimization of transfection conditions increased rAAV titer up to ∼50%, and thus provided a platform to scrutinize the proteomic landscape of HEK293T cells with differential rAAV yields.

Development of a spectral library utilizing HEK293T cell line for AAV2 production

The HEK293T global spectral library was constructed with data from a total of 72 data-dependent acquisition (DDA) runs. MS/MS spectra data were acquired from both untransfected and rAAV2-producing HEK293T cell lines, comprising whole-cell lysate; subcellular lysate of nuclear, mitochondrial, and membrane protein fractions; and high-pH (basic) reversed-phase (bRP) peptide fractions from untransfected cells, as well as whole-cell lysates and bRP peptide fractions from all transfected rAAV2-producing cell populations (Figure 2). Default Spectronaut Pulsar settings, a 1% false discovery rate (FDR) cutoff at the peptide and protein level, and a minimum requirement of two unique peptides per protein were applied in the curation of the HEK293T spectral library. Improved proteome coverage was achieved with increased fractionation, resulting in the identification of 1,430 protein groups in the cell lysate (CL), 3,750 protein groups in CL and subcellular lysate (SL), 6,277 protein groups in bRP-fractionated CL/SL, and a total of 7,183 protein groups in the combined global library (Figure 2B). Functional annotation using the PANTHER database revealed that a significant portion of the library's proteins are associated with fundamental biological processes, including cellular processes, biological regulation, and metabolic processes (Figure 2C). Additionally, our spectral library consists of proteins well-distributed across various cellular components, ranging from cytosolic fractions to cellular organelles, thus representing a diverse protein landscape within the cell.

The integration of data from AAV-producing cells into our spectral library will also improve representation of the dynamic proteome landscape associated with AAV production, and thus generate a tailored spectral library that is potentially better optimized for the study of AAV production in HEK293T cells compared with previously reported pan-human spectral libraries generated using untransfected cells.[19]

Profiling the whole-cell proteome of HEK293T-AAV transfectants

In this investigation, we utilized the SWATH-MS-based label-free quantification methodology to conduct a comparative analysis of the proteome profiles among HEK293T-AAV transfectants exposed to three distinct conditions: the standard, sub-optimal, and optimal conditions. To enhance our analytical capabilities for label-free quantification, we constructed a curated spectral library using untransfected and rAAV2-producing HEK293T cell lines. This

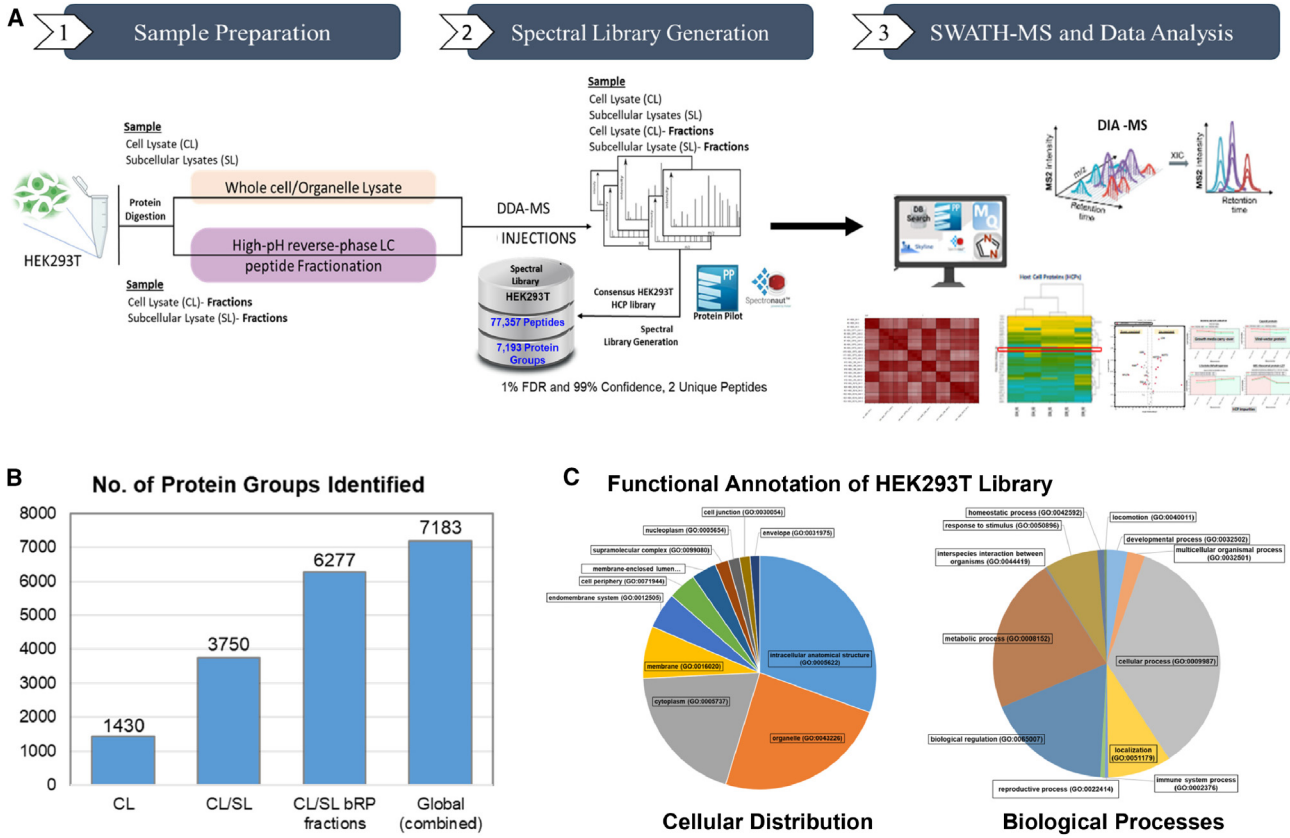

Figure 2. Comprehensive spectral library for the analysis of the HEK293T proteome by SWATH-MS

(A) Workflow for the construction and use of the HEK293T global spectral library. HEK293T cells were lysed and fractionated using differential ultracentrifugation to obtain nuclear, mitochondrial, and membrane protein fractions. Tryptic digest of cell lysate (CL) and subcellular lysate (SL) were further fractionated by high-pH (basic) reversed-phase (bRP) chromatography. All CL, SL, and bRP-fractionated CL/SL samples were subjected to DDA-MS analysis and processed using ProteinPilot and Spectronaut Pulsar software for the construction of the spectral library. The applicability and robustness of the HEK293T global spectral library were evaluated with SWATH-MS datasets obtained from different project-independent AAV-producing HEK293T samples and various LC-MS instrumental setups (data not included). (B) Bar graph showing increasing proteome depth with fractionation in the construction of a comprehensive spectral library for HEK293T cell line. DDA files were processed using ProteinPilot, with the following filter parameters applied: Peptide −10logP ≥ 15, protein group FDR of 1.0%, and proteins unique peptides ≥ 2. (C) Pie charts showing the distribution of the cellular components and biological processes of identified proteins in the HEK293T global spectral library. The distribution of GO terms was categorized based on PANTHER GO-Slim.

comprehensive proteome profiling was performed at multiple time points, specifically at 24, 48, and 72 h post-transfection (hpt), across all transfection conditions. Consistent identification of approximately 4,000 protein groups was achieved, with a stringent FDR of <0.01 (Figure 3B; Tables S1 and S2). The proteomes from all samples were analyzed using three-dimensional principal-component analysis (PCA), which revealed that the proteomes clustered together at the early infection time point of 24 hpt and diverged increasingly with time.

Proteomic analysis of HEK293T producer cell line under optimal transfection condition

Optimal condition exhibited the highest rAAV titer at 72 hpt compared with standard and sub-optimal transfection conditions, with a 50% increase in titer compared with the standard transfection condition (Figure 1B). Our central focus thus revolves around the elucidation of the molecular and functional transformations associated with the optimal transfection condition. Our proteome analysis, executed under this specific transfection condition, enabled the identification and quantification of 4,741 protein groups with FDR ≤0.01 (Figure 3B). At each time point (24, 48, and 72 hpt), we identified sets of differentially expressed proteins, characterized by fold changes of at least 1.5 ($p \leq 0.05$). In comparison with the standard transfectants, we observed an increase in the abundance of 74 proteins at 24 hpt, 146 proteins at 48 hpt, and 133 proteins at 72 hpt (Figures 4, 5, and 6A, Table S1). Simultaneously, we observed a decrease in the abundance of 102 proteins in optimal transfectants at 24 hpt, 108 proteins at 48 hpt, and 411 proteins at 72 hpt, corresponding to the progression of rAAV production.

We conducted functional enrichment analysis on the subset of differentially expressed proteins across all time points, with the results

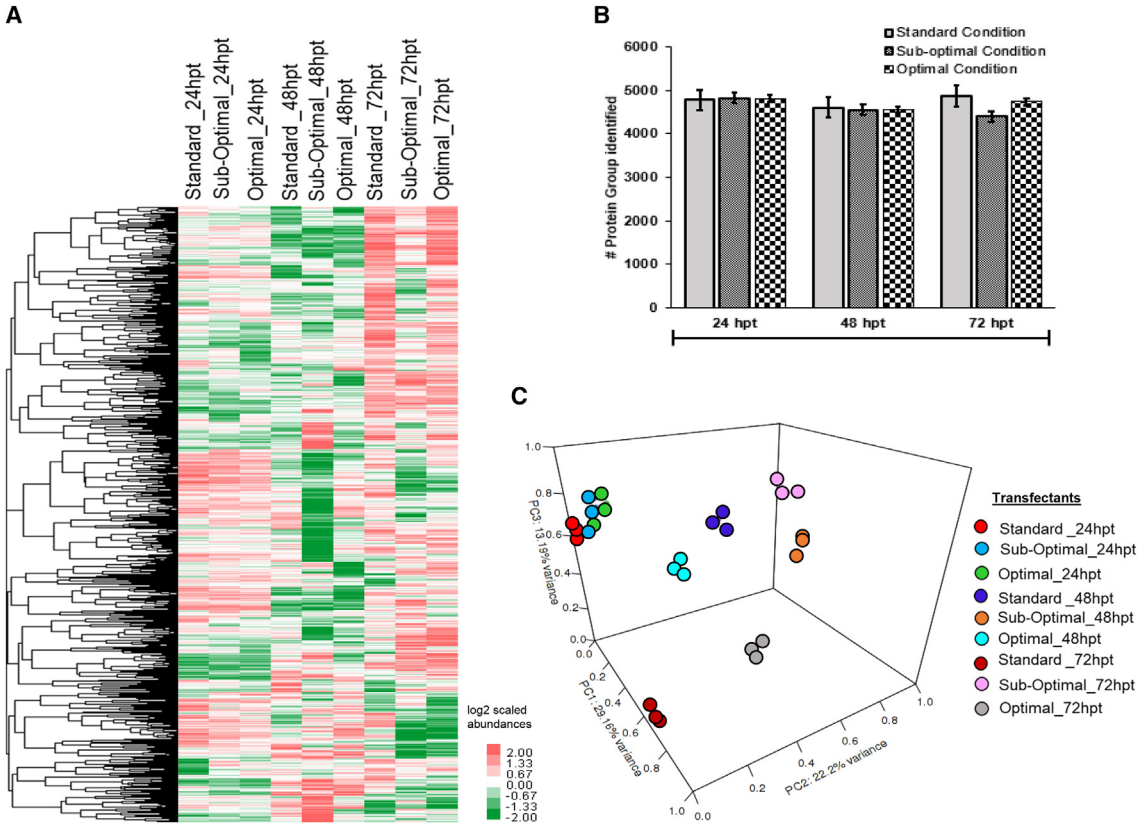

Figure 3. Comparative proteomic analysis of rAAV-producing HEK293T transfectants at different time points

(A) Hierarchically clustered heatmap of scaled protein abundances in HEK293T-AAV transfectants at different time points (24, 48, and 72 hpt); protein groups with missing values were excluded. The hierarchical clustering was generated using the neighbor-joining algorithm, with a Euclidean distance similarity measurement of the log2 ratios of the abundance of each sample relative to the average abundance of all samples. (B) Total number of protein groups detected in HEK293T-AAV transfectants (subjected to standard, sub-optimal, or optimal transfection conditions) at different time points post-transfection. (C) Principal-component analysis (PCA) of the triplicate proteomics datasets from the HEK293T-AAV transfectants.

presented in Table S3. During the initial stages of AAV production at 24 hpt, various Gene Ontology (GO) biological processes and Kyoto Encyclopedia of Genes and Genomes (KEGG) pathways displayed distinctive regulation patterns (Figure 4). Specifically, upregulated processes included Golgi vesicle-mediated transport (e.g., EXOC4, CCDC93, EPS15, EXtoOC2, VTI1B), RNA metabolism (e.g., RNGTT, PCBP2, LAGE3), regulation of the cell cycle (e.g., HMGA2, TP53, UCHL5, SIRT2, MAP2K6), fatty acid biosynthesis (e.g., ERLIN1, SIRT2), and cellular stress responses (e.g., DNAJB6, NUP85, NUP42, HSPA6). We also identified five interconnected pathways: "Cellular Response to Heat Stress," "Cell Cycle, Mitotic," "Metabolism of RNA," "Viral Infection," and "Transport of Ribonucleoproteins." Common upregulated proteins, such as NUP42 and NUP85, are essential components of the nuclear pore complex. Their upregulation provides additional evidence supporting the facilitation of nuclear import of AAV particles or viral components, potentially impacting viral replication or gene expression.[20–24] Additionally, several other biosynthetic pathways were upregulated, such as oligosaccharide-lipid intermediate processes (e.g., ALG12, MPDU1), cellular lipid biosynthesis, and glycerol ether biosynthesis (e.g., FAR1, ERLIN1) at 24 hpt. In parallel, downregulated GO biological processes included DNA-templated transcription (e.g., MAZ, SSU72), autophagy (e.g., MTMR9, FOXK1, ATP6V1C1), cellular localization, and ubiquitin protein-dependent catabolic processes (e.g., UBE2C, RNF25, FBXO7). Downregulated KEGG pathways included pyrimidine metabolism (e.g., TK1, DCK), homeostasis (e.g., FTH1, ATP6V1C1, FTL), membrane trafficking (e.g., KLC4, DCTN5, TBC1D13, CLTB, COPS7A, ARF5, KIF15), mitochondrial biogenesis (e.g., UBE2C, UBE2E3), and vesicle-mediated transport proteins related to interleukin signaling pathways (e.g., IL-2 and IL-5).

AAV production is a complex process involving multiple steps. After transfection, the viral DNA needs time to replicate within the host cell. This replication process usually takes several hours. Additionally, the viral components need to be assembled into functional AAV particles. This assembly process also takes time. By 48 hpt, both replication and assembly have likely progressed significantly compared with

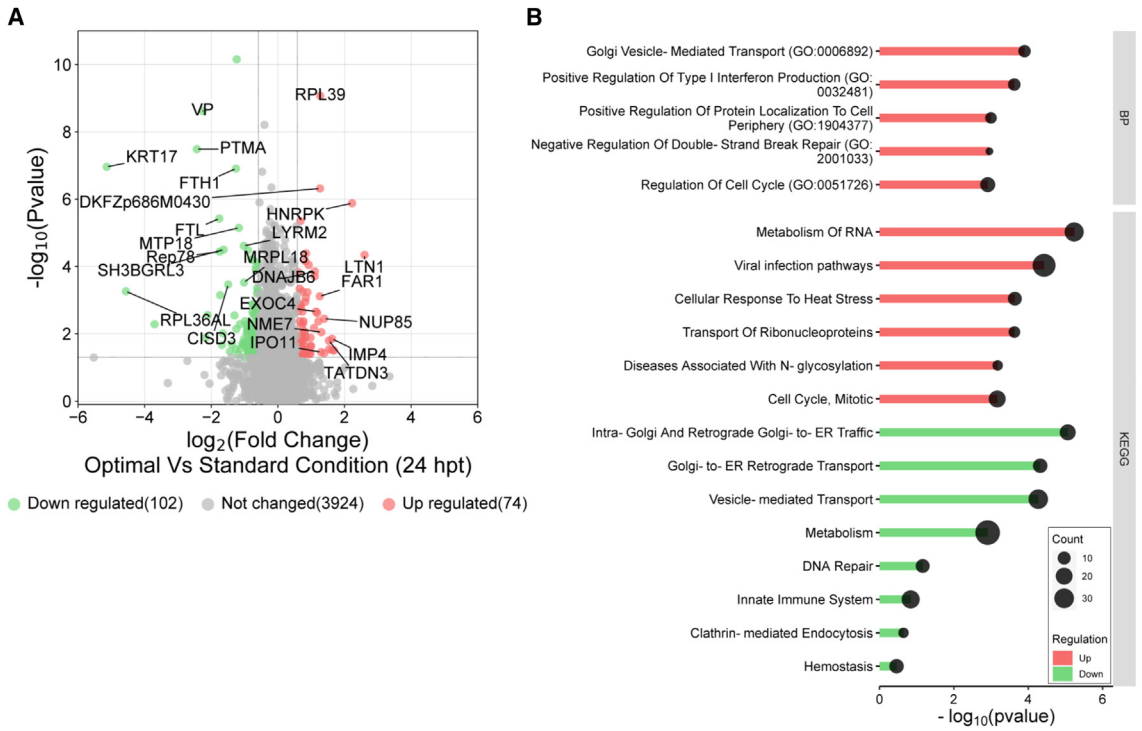

Figure 4. Analysis of differentially expressed proteins in optimal vs. standard transfectants at 24 hpt

(A) Volcano plot of log2 fold change against associated −log10 *p* value. Cutoffs applied correspond to *p* value of 0.05, and fold change of 0.5 and 2, with significantly differentially expressed proteins (DEPs) shaded in red (upregulated) or green (downregulated). (B) Enrichr enrichment analysis of DEPs revealed enriched GO biological processes and KEGG pathways in optimal transfectants compared with standard transfectants at 24 hpt.

24 hpt. We observed a substantial increase in the expression of viral proteins at 48 hpt compared with 24 hpt (Figures S1 and S2). This heightened expression coincided with the upregulation of various GO biological processes and KEGG pathways. These included cell division, DNA-templated transcription, homeostasis, viral RNA transcription, cytoskeleton organization, metabolic processes involving organonitrogen compounds, catabolic processes dependent on ubiquitin proteins, ribosomal biogenesis, cellular localization, and catabolic processes (Figure 5). Furthermore, we observed a downregulation in the generation of metabolites, energy production, carboxylic acid biosynthesis, mitochondrial ATP synthesis coupled with electron transport, and cellular catabolic processes. Additionally, specific cellular protein complexes, including MRE11, BRCA1-C, oxidoreductases, and other mitochondrial protein complexes, exhibited a reduction in their expression levels.

At 72 hpt, we noted changes associated with specific GO molecular functions, including increased activities of oxidoreductases, nucleosomal binding proteins, and acyl-CoA dehydrogenases (Figure 6). Additionally, GO biological processes such as mitochondrion organization, cellular lipid metabolism, biosynthesis of organonitrogen compounds, formation of DNA packaging complexes, stress responses, and apoptosis pathways were upregulated. Viral replication and the high metabolic demands of viral protein synthesis can lead to cellular stress and potentially trigger cell death pathways. Additionally, the release of large quantities of viral particles during the late stages of infection can cause cell lysis, leading to cell death.[25] Consequently, biological processes such as cell cycle/division, cellular regulations, translation, ribosomal biogenesis, chromosome segregation, and vesicle budding were all downregulated. Additionally, KEGG pathways such as ubiquitin-mediated proteolysis and other signaling pathways experienced downregulation. Mitochondrial and membrane-bound proteins were also downregulated within cellular components at this stage of the culture time.

Protein-protein interaction network reveals role of HEK293T proteins in AAV replication, assembly, and protein synthesis

Our investigation showed dynamic regulation of the host proteome, which plays a pivotal role in governing the processes of AAV2 replication, assembly, and protein expression. From an extensive review of existing literature[20–23,26] and the VirHostNet 2.0 database,[24,27] we identified a subset of 124 differentially expressed host proteins associated with virus-host interactions in optimal transfectants compared with standard transfectants in at least one post-transfection time point assessed (Table S4).

To gain a more profound understanding of the functional implications of these proteins, we employed Protein-Protein Interaction

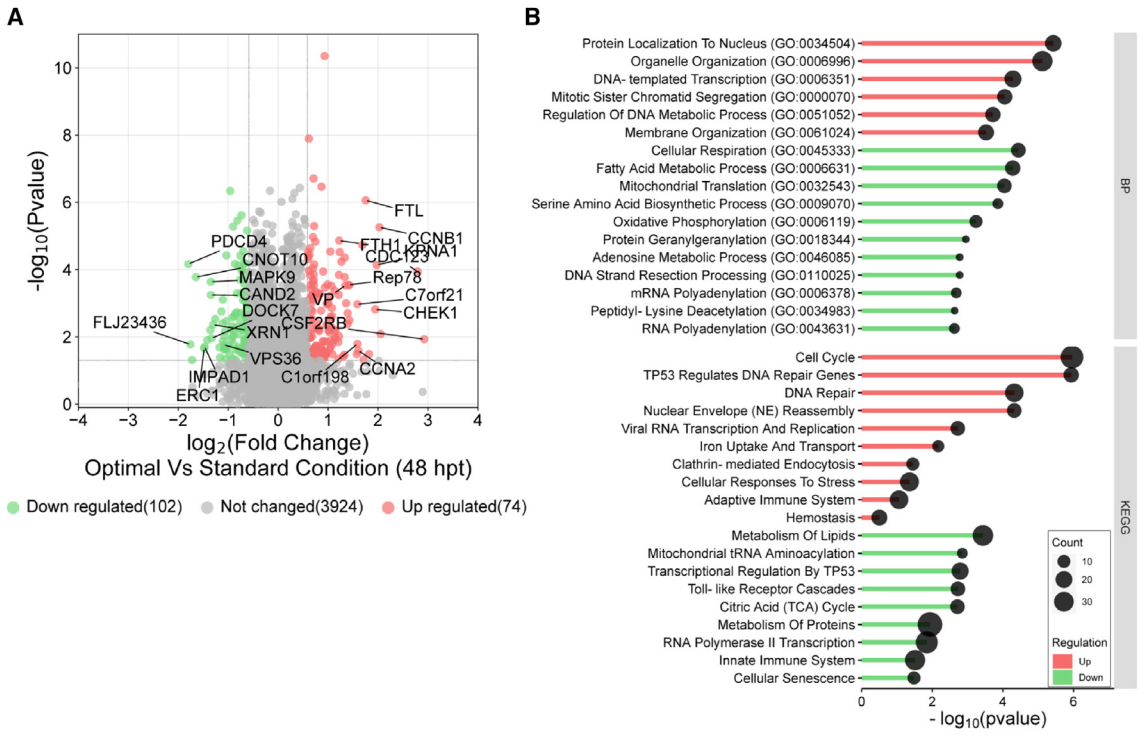

Figure 5. Analysis of differentially expressed proteins in optimal vs. standard transfectants at 48 hpt

(A) Volcano plot of log2 fold change against associated −log10 *p* value. Cutoffs applied correspond to *p* value of 0.05, and fold change of 0.5 and 2, with significantly differentially expressed proteins (DEPs) shaded in red (upregulated) or green (downregulated). (B) Enrichr enrichment analysis of DEPs revealed enriched GO Biological Processes and KEGG pathways in optimal transfectants compared with standard transfectants at 48 hpt.

Network Functional Enrichment Analysis using full STRING network settings (indicating both functional and physical protein associations). Subsequently, we applied K-means clustering with a stringent confidence threshold of 0.700, which categorized these proteins into seven unique clusters (Figure 7). These seven clusters comprised 92 proteins (Tables 1 and S4) and revealed associations with functional enrichment in specific pathways. These pathways encompassed viral entry into host (GO: 0075506); viral protein processing, modulation, and replication (GO: 0051851); autophagy (GO: 0010506); viral life cycle/ECRT complex (GO: 0019058/0039702); peptidyl-proline modification (cell signaling) (GO: 0018208); viral translational termination-reinitiation (GO: 0075522); and host-enhanced viral transcription (GO: 0043923). Notable examples include DNA repair proteins like MRE11 and RAD50, which played a role in negatively regulating viral entry into the host cell (GO: 0075506).

In this study, we identified an enrichment in processes related to IRES-dependent viral translational initiation and the endosomal sorting complex required for transport (ESCRT) complex, well-known for its involvement in cellular budding. This enrichment stemmed from the differential expression observed in a cluster of proteins, including charged multivesicular body proteins (CHMP1A, CHMP1B, CHMP2A, CHMP2B, CHMP4B, CHMP5, and CHMP6), vesicle-associated membrane proteins (VAPA, VPS4A, VPS4B, and VAPB), and other significant proteins like acuolar protein sorting-associated protein (IST1), tumor susceptibility gene 101 (TSG101), valosin-containing protein (VCP), TAR DNA-binding protein (TARDBP), and proteasome subunit beta, type 4 (P4HB). The cluster associated with viral translational termination-reinitiation processes exhibited regulatory control by protein families, including eukaryotic translation initiation factors, poly(rC)-binding protein 1 (PCBP1), density-regulated protein (DENR), synaptic functional regulator (FMR1), and malignant T cell-amplified sequence 1 (MCTS1), among others.

Our enrichment analysis further highlighted the differential expression of proteins involved in host cell signaling, encompassing peptidyl-prolyl *cis*-trans isomerases (PPIA, PPIB, and PPID), cofilin, non-muscle isoform (CFL1), high-mobility group protein 1 (HMGB1), and profilin-1 (PFN1). The observed variations in protein expression across these seven clusters collectively signify that, at 48 hpt, there is a notable increase in the abundance of host proteins that are found at lower levels during the early and late stages of intracellular viral production (Figure 7).

DISCUSSION

This study aimed to understand the molecular and biological processes in HEK293T cells during rAAV2 production using the

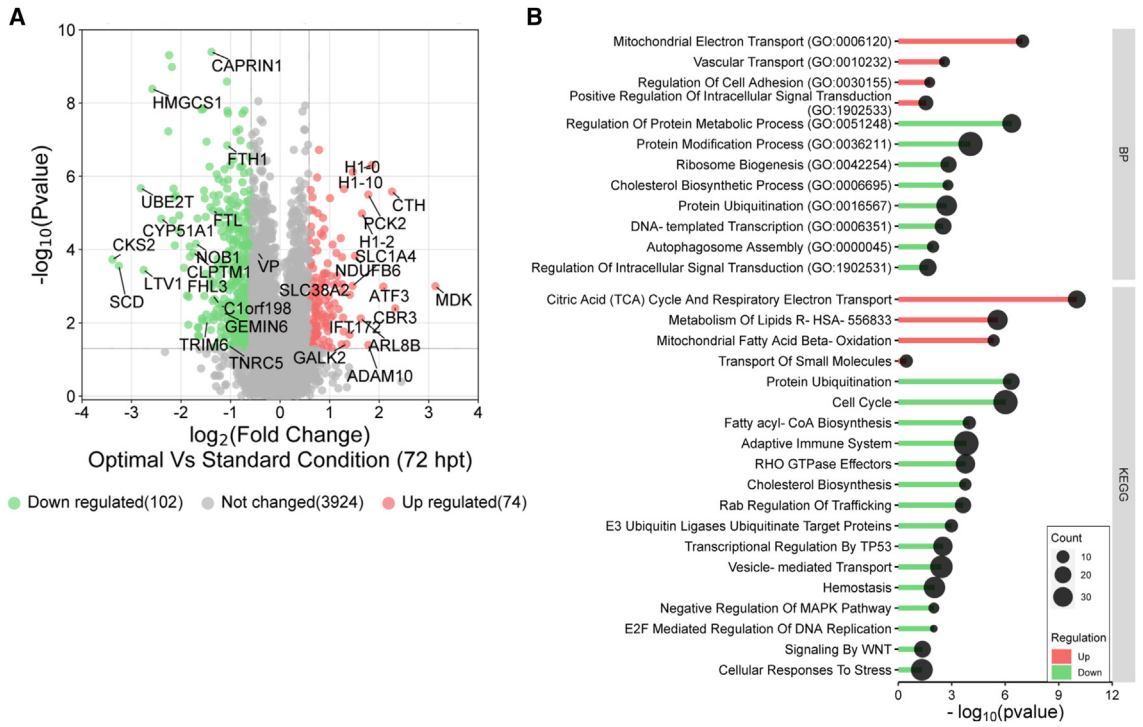

Figure 6. Analysis of differentially expressed proteins in optimal vs. standard transfectants at 72 hpt

(A) Volcano plot of log2 fold change against associated −log10 *p* value. Cutoffs applied correspond to *p* value of 0.05, and fold change of 0.5 and 2, with significantly differentially expressed proteins (DEPs) shaded in red (upregulated) or green (downregulated). (B) Enrichr enrichment analysis of DEPs revealed enriched GO Biological Processes and KEGG pathways in optimal transfectants compared with standard transfectants at 72 hpt.

SWATH-MS method. Previous studies have primarily focused on comparing untransfected (control) and transfected (GFP-expressing) HEK293 cells at 72 hpt.[17,18] Here, we utilized the SWATH-MS method to evaluate the temporal changes in proteome profiles associated with varying titers of rAAV production under three distinct transfection conditions—standard, sub-optimal, and optimal—in HEK293T cells. SWATH-MS is particularly well-suited for this study due to its ability to provide comprehensive and quantitative proteome coverage, enabling the precise characterization of the temporal dynamics of protein expression during rAAV production. Applying SWATH-MS, together with a comprehensive spectral library of 7,183 protein groups constructed from both untransfected and rAAV-producing HEK293T cells, has allowed us to delve into the intricate processes underlying rAAV production and contributes to a deeper understanding of the factors influencing enhanced rAAV bioprocessing efficiency under optimal transfection conditions.

Differential expression analysis shed light on the dynamic alterations in protein levels during rAAV production. Specifically, at 24 hpt, various biological processes and pathways associated with cellular processes, RNA metabolism, and cell cycle regulation exhibited upregulation. Conversely, pathways related to DNA-templated transcription, autophagy, and ubiquitin protein-dependent catabolic processes were downregulated. We compared the transcriptional data previously reported[28–32] with our proteomics data, wherein we found five proteins, Tetraspanin (CD81), ATPase H(+)-transporting lysosomal accessory protein 2 (ATP6AP2), Plasmalemma vesicle-associated protein (PLVAP), Disks large homolog 1 (DLG1), and WD repeat-containing protein 54 (WDR54), associated with the regulation of MAPK cascade that were similarly downregulated at early time points.

At 48 hpt, increased viral protein coincided with upregulation of proteins responsible for cell division, protein ubiquitination, DNA-templated transcription, homeostasis, and various metabolic processes. Notably, proteins involved in ubiquitin ligases and ferritin complexes displayed high abundance. Although host cells use ubiquitination to target and degrade incoming pathogens as a defense mechanism, viruses have evolved to exploit this process. Viruses can hijack the ubiquitin system to augment different stages of their replication cycle and enhance pathogenesis.[33,34] Our data also revealed a significant upregulation of EIF2 signaling (EIF2B2, EIF2D), oxidative phosphorylation, and the spliceosomal cycle in optimal transfectants compared with standard transfectants. EIF2 is pivotal in governing protein synthesis in eukaryotic cells.[20,35,36] Furthermore, EIF2 activation, typically induced by phosphorylation, acts as a cellular stress response, especially in the context of viral infections. We also observed increased expression of host cell proteins associated with import pathways, potentially indicating enhanced transport of viral components needed for replication and assembly is required for higher

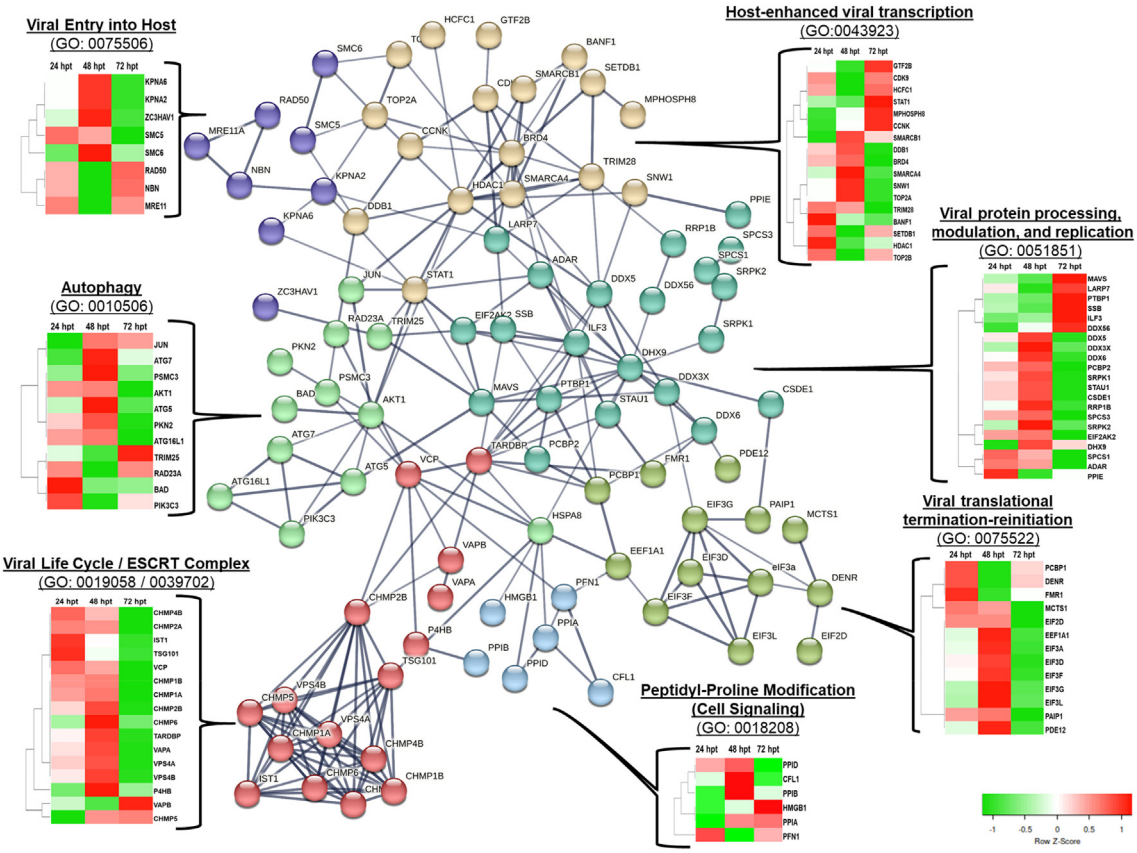

Figure 7. Proteins associated with AAV replication and assembly: temporal protein-protein interactions in HEK293T cells

Lines connecting proteins represent experimentally validated protein-protein interactions (PPIs), highlighting their intricate interplay during rAAV viral production. Heatmaps depict protein abundance levels at distinct time points (24, 48, and 72 hpt), providing valuable insights into the regulation of AAV production (data shown for optimal transfection condition).

rAAV productivity (Figures 4, 5, and 6 and Table S3). Importin proteins such as KPNA2, KPNA1 may facilitate the nuclear import of these viral replication proteins, allowing them to carry out their functions in the nucleus.[37–40] Importins are critical for rAAV by enabling the viral DNA to enter the nucleus, the essential first step for replication and subsequent packaging of functional rAAV particles. This aligns with the established role of AAV-encoded replication proteins in processes like DNA replication and transcription, highlighting the intricate interplay between host and viral factors during rAAV production.

At 72 hpt, differential proteomic analysis revealed several upregulated activities, including oxidoreductase activities, nucleosomal binding, and acyl-CoA dehydrogenase activities. These findings suggest an increase in metabolic activity and potential adaptation to viral replication. Proteins associated with the electron transport chain, tricarboxylic acid (TCA) cycle, mitochondrial complex I, and cellular lipid metabolism showed elevated expression levels (Table S3). Given their fundamental roles in cellular metabolism, alterations in the abundance of these proteins may significantly affect overall cellular processes, potentially impacting factors critical to rAAV production.[41] Conversely, there was a downregulation in cellular processes such as fatty acid and cholesterol biosynthesis, cell cycle/division, translation, and vesicle budding pathways (Table S3). Fatty acids play an important role in viral assembly and vesicle budding,[42] whereas, modulation of host-cholesterol facilitates viral entry, replicative complexes formation, assembly, egress, and control of the interferon type I response in *Flavivirus* spp.[43] This downregulation, particularly of fatty acids, could be a host defense mechanism to restrict viral assembly and the role of cholesterol in AAV infection remains to be elucidated, although its importance in *Flavivirus* suggests a potential role.

Innate immune response pathways are known to be activated upon detection of E2A, E4, and VA RNA encoded by pHelper plasmid.[44–46] These adenovirus helper functions play a vital role in supporting the AAV life cycle, encompassing processes like replication and packaging. In response to the detection of viral components within HEK293 cells, there is often an activation of Innate Immune Response Pathways. While the primary objective of the innate immune response is to eradicate viruses, its activation can have adverse effects

Table 1. Functionally enriched pathways and HEK293T host cell genes/proteins implicated in viral replication, assembly, and protein expression

Functional enrichment	Gene ID	Name
Autophagy (GO: 0010506)	JUN	Transcription factor AP-1
	ATG7	Ubiquitin-like modifier-activating enzyme ATG7
	PSMC3	26S proteasome regulatory subunit 6A
	AKT1	RAC-alpha serine/threonine-protein kinase
	ATG5	Autophagy protein 5
	PKN2	Serine/threonine-protein kinase N2
	ATG16L1	ATG16 autophagy-related 16-like 1
	TRIM25	E3 ubiquitin/ISG15 ligase TRIM25
	RAD23A	UV excision repair protein RAD23
	BAD	BCL2-antagonist of cell death, isoform CRA_c
	PIK3C3	Phosphatidylinositol 3-kinase catalytic subunit type 3
Viral entry into host (GO: 0075506)	KPNA6	Importin subunit alpha-7
	KPNA2	Importin subunit alpha-1
	ZC3HAV1	Zinc finger CCCH-type antiviral protein 1
	SMC5	Structural maintenance of chromosomes protein 5
	SMC6	Structural maintenance of chromosomes 6
	RAD50	DNA repair protein RAD50
	NBN	Nibrin
	MRE11	MRE11 homolog, double-strand break repair nuclease
Viral protein processing, modulation, and replication (GO: 0051851)	MAVS	Mitochondrial antiviral-signaling protein
	LARP7	La-related protein 7
	PTBP1	Polypyrimidine tract-binding protein 1
	SSB	Autoantigen La (Fragment)
	ILF3	Interleukin enhancer binding factor 3, 90kDa, isoform CRA_d
	DDX56	RNA helicase (Fragment)
	DDX5	DEAD box protein 5 (Fragment)
	DDX3X	RNA helicase
	DDX6	Probable ATP-dependent RNA helicase DDX6
	PCBP2	Poly(rC)-binding protein 2
	SRPK1	SRSF protein kinase 1 (Fragment)
	STAU1	Double-stranded RNA-binding protein Staufen homolog 1
	CSDE1	Cold shock domain-containing E1, RNA-binding
	RRP1B	Ribosomal RNA processing protein 1 homolog B
	SPCS3	Signal peptidase complex subunit 3
	SRPK2	SFRS protein kinase 2
	EIF2AK2	Interferon-induced, double-stranded RNA-activated protein kinase
	DHX9	ATP-dependent RNA helicase A
	SPCS1	Signal peptidase complex subunit 1
	ADAR	Double-stranded RNA-specific adenosine deaminase
	PPIE	Peptidyl-prolyl *cis*-trans isomerase E

(*Continued on next page*)

Table 1. *Continued*

Functional enrichment	Gene ID	Name
Viral life cycle/ECRT complex (GO: 0019058/ 0039702)	CHMP4B	Charged multivesicular body protein 4b
	CHMP2A	Chromatin modifying protein 2A, isoform CRA_b
	IST1	IST1 homolog
	TSG101	Tumor susceptibility gene 101 protein
	VCP	Transitional endoplasmic reticulum ATPase
	CHMP1B	Charged multivesicular body protein 1b
	CHMP1A	Charged multivesicular body protein 1a
	CHMP2B	Charged multivesicular body protein 2b
	CHMP6	Charged multivesicular body protein 6 (Fragment)
	TARDBP	TAR DNA-binding protein 43
	VAPA	Vesicle-associated membrane protein-associated protein A
	VPS4A	Vesicle-fusing ATPase 4A
	VPS4B	Vesicle-fusing ATPase 4B
	P4HB	Protein disulfide-isomerase
	VAPB	Vesicle-associated membrane protein-associated protein B/C
	CHMP5	Charged multivesicular body protein 5
Peptidyl-proline modification (Cell Signaling) (GO: 0018208)	PPID	Peptidyl-prolyl *cis*-trans isomerase D
	CFL1	Cofilin, non-muscle isoform
	PPIB	Peptidyl-prolyl *cis*-trans isomerase B
	HMGB1	High-mobility group protein 1
	PPIA	Peptidyl-prolyl *cis*-trans isomerase
	PFN1	Profilin-1
Viral translational termination-reinitiation (GO: 0075522)	PCBP1	Poly(rC)-binding protein 1
	DENR	Density-regulated protein
	FMR1	Synaptic functional regulator FMR1
	MCTS1	Malignant T-cell-amplified sequence 1
	EIF2D	Eukaryotic translation initiation factor 2D
	EEF1A1	Elongation factor 1-alpha 1
	EIF3A	Eukaryotic translation initiation factor 3 subunit A
	EIF3D	Eukaryotic translation initiation factor 3 subunit D
	EIF3F	Eukaryotic translation initiation factor 3 subunit F
	EIF3G	Eukaryotic translation initiation factor 3 subunit G
	EIF3L	Eukaryotic translation initiation factor 3 subunit L
	PAIP1	Polyadenylate-binding protein-interacting protein 1
	PDE12	2′,5′-phosphodiesterase 12
Host-enhanced viral transcription (GO: 0043923)	GTF2B	Transcription initiation factor IIB
	CDK9	Cyclin-dependent kinase 9
	HCFC1	Host cell factor 1
	STAT1	Signal transducer and activator of transcription
	MPHOSPH8	M-phase phosphoprotein 8
	CCNK	Cyclin K, isoform CRA_c
	SMARCB1	

(*Continued on next page*)

Table 1. *Continued*

Functional enrichment	Gene ID	Name
		SWI/SNF-related matrix-associated actin-dependent regulator of chromatin subfamily B member 1
	DDB1	DNA damage-binding protein 1
	BRD4	Bromodomain-containing protein 4
	SMARCA4	Transcription activator BRG1
	SNW1	SNW domain-containing protein 1
	TOP2A	DNA topoisomerase 2-alpha
	TRIM28	Transcription intermediary factor 1-beta
	BANF1	Barrier to autointegration factor 1, isoform CRA_a
	SETDB1	Histone-lysine N-methyltransferase SETDB1
	HDAC1	Histone deacetylase 1
	TOP2B	DNA topoisomerase 2-beta

on AAV production in HEK293 cells, leading to a reduction in viral replication. Prolonged or excessive activation of the innate immune response is also known to induce apoptosis in HEK293 cells, ultimately diminishing overall production. While conventional transfection protocols in HEK293 cells often elicit an upregulated immune response,[44–46] our optimal transfection condition led to a notable downregulation or reduced expression of proteins associated with the immune response, including ASAH1, CREB1, CD81, POLR3F, STOM, ATP11B, ATP6V1C1, and NFKB2 (Table S3), in comparison with the standard transfection condition.[47–51] This indicates that the host immune response modulation may potentially contribute to viral production yield.

AAV viral production cycle is critically dependent on the cellular replication and translation apparatus of the host cell. Given that viral proteins and viral nucleic acids are perceived as exogenous entities within the host cell milieu, their presence has the potential to trigger a series of host cell stress reactions, including but not limited to autophagy, endoplasmic reticulum stress, and programmed cell death (apoptosis).[52] Our investigation unveiled increased activation of these stress responses associated with viral production (Figures 4, 5, and 6).[17,47,53–56] Tables S3 and S4 provide details of GO enrichment results and log2 FC values for all the time points post-transfection for the optimal transfection condition and list of host cell proteins directly associated with viral replication and production.

A subsequent refined focus toward 124 host proteins was taken based on the biocuration reports of VirHostNet database on proteins exhibiting unique expression patterns during viral production, including rAAV. Functional enrichment analysis and K-means clustering using STRING-DB effectively categorized these proteins into seven distinct clusters, each closely link to distinct pivotal processes like viral entry into host, "viral protein processing, modulation, and replication," autophagy, viral life cycle/ESCRT complex, peptidyl-proline modification, viral translational termination-reinitiation, and host-enhanced viral transcription.

Distinctive expression patterns of the ESCRT pathway were found in optimal transfectants compared with standard transfectants (Table S3). The ESCRT machinery played multifaceted roles in various fundamental cellular processes, including cell cytokinesis, organelle and vesicle biogenesis, maintenance of nuclear-cytoplasmic compartmentalization, and endolysosomal activity,[57–59] and has a critical role in AAV production by facilitating capsid budding and scission, regulating viral protein turnover, and potentially contributing to viral genome packaging.[60–68] The core ESCRT machinery comprises three essential complexes, namely ESCRT-I, ESCRT-II, and ESCRT-III, along with the AAA-type ATP-ase (ATPases associated with diverse cellular activities), vacuolar protein sorting (VPS4 proteins). Our investigation revealed variations in the expression levels of proteins within the CHMP family, such as CHMP1B, CHMP1A, CHMP2A, CHMP2B, CHMP4B, CHMP5, and CHMP6. Specifically, these proteins were found to be upregulated during peak rAAV production under optimal transfection conditions at 48 hpt.[69,70] These proteins play pivotal roles in processes such as endosomal sorting, multivesicular body (MVB) formation, and the budding of viruses, each contributing distinct functions within the ESCRT pathway.[63,71–76]

Interestingly, AAV also appears to exploit autophagy to aid in its escape from endosomes.[77,78] The autophagy machinery, including components like autophagy-related proteins (ATGs), was utilized by AAV to facilitate its transport from endosomes to the cytoplasm, where it can initiate productive infection (Table S3).

Certain peptidyl-proline modifications are known to play crucial roles in cell signaling pathways. In our study, we identified several key proteins, including peptidyl-prolyl *cis*-trans isomerases (PPIA, PPIB, and PPID), profilin-1 (PFN1), cofilin-1 (CFL1), and high-mobility group

protein B1 (HMGB1), which were differentially regulated in a temporal manner (Figure 7). These proteins have been previously implicated in facilitating AAV replication and packaging processes. PPIA, PPIB, and PPID catalyze the isomerization of peptidyl-prolyl bonds, influencing the folding, stability, and activity of proteins involved in viral replication.[78] Furthermore, profilin-1 (PFN1) and cofilin-1 (CFL1) may modulate actin dynamics critical for the intracellular transport of viral components during AAV vector assembly and packaging.[79]

In summary, this study offers a comprehensive analysis of the dynamic proteome changes associated with different AAV production titers, providing valuable insights for potential applications in AAV bioprocessing. By elucidating the temporal changes in host cell protein function, this study provides insights into the dynamic remodeling of the host proteome during AAV production. These findings not only lay the groundwork for enhancing the efficiency of viral vector production but also underscore the potential for optimizing plasmid molar ratios and designing improved HEK293T cell lines. With this knowledge, we can develop enhanced transient transfection conditions to achieve higher yields of AAV and other viral vectors, thus benefiting a wide array of applications.

MATERIALS AND METHODS

Ethics statement

All experiments were conducted in accordance with the approved guidelines of the Bioprocessing Technology Institute (BTI), Agency for Science, Technology and Research (A*STAR), Singapore.

Experimental design

In order to conduct functional and molecular characterization studies on various transient transfection conditions in the HEK293T cell line responsible for AAV2 production, we employed label-free quantitative proteomics using the SWATH-MS method with a peptide-centric data analysis approach.[80] This study investigated three distinct triple transfection conditions for AAV2 production in HEK293T cells. These conditions included a standard condition (with a defined pHelper: pAAV_RC2: pAAV_GFP ratio of 1:1:1) and two additional conditions designated as sub-optimal and optimal (plasmid ratios undisclosed for proprietary reasons). All transfections were performed at a cell density of $1 \times 10\text{^}6$ cells/mL for the standard condition, while a higher cell density of $2.5 \times 10\text{^}6$ cells/mL was used for both the sub-optimal and optimal conditions. Samples were collected at three time points post-transfection: 24 h post-transfection (hpt), 48 hpt, and 72 hpt. To ensure robust protein identification and consistent quantification using SWATH-MS, a comprehensive spectral library specific to the HEK293T cell line used in AAV production was meticulously constructed (Figure 2). Following deconvolution and spectral matching, a variety of statistical analyses were performed.

rAAV production

In-house suspension-adapted HEK293T (ATCC) was transfected using pHelper, pAAV_RC2, and pAAV_GFP plasmids (CellBiolabs, VPK-402). Transfection was performed using PEI MAX (Polysciences, Inc). Cells were cultured in F17 (Thermo Fisher Scientific, A1383501) medium supplemented with 8 mM L-glutamine (Thermo Fisher Scientific, 25030081) and 0.1% Pluronic-F68 (Thermo Fisher Scientific, 24040032). Cells were harvested for titering 72 h post-transfection.

rAAV titering

Cells were lysed and lysates were processed as described by Grieger et al.[81] rAAV titering was performed on crude cell lysates using dye-based qPCR (NEB, M3003L) with primers against ITR regions. ITR primer sequences were obtained from Aurnhammer et al.[82] Linearized plasmid standards were obtained by digesting pAAV_GFP with HindIII restriction enzyme (NEB, R3104S).

Sample preparation

The cell pellet was lysed in lysis buffer (5% SDS in 50 mM TEAB, pH 8.5 with benzonase) and clarified by centrifugation. Protein concentration was determined using the Pierce BCA Protein Assay kit (Thermo Fisher Scientific). A total of 100 μg of protein lysate was reduced and alkylated, then trypsin-digested overnight at 37°C on an S-Trap mini spin column (ProtiFi) following the manufacturer's protocols. Eluted peptides were dried and reconstituted in loading buffer (1% formic acid in 2% acetonitrile) for mass spectrometry analysis.

Construction of HEK293T spectral library generation

Lysate, subcellular fractions, and high-pH reversed-phase fractionated samples from both untransfected and rAAV2-producing HEK293T cell lines were analyzed using a TripleTOF 6600 mass spectrometer in DDA mode, as previously described. A total of 72 raw DDA data files were processed using ProteinPilot software (version 5.0.2, SCIEX) and Spectronaut Pulsar for HEK293T spectral library construction. Protein identification was performed against the human UniProt reference proteome database (downlaoded in September 2021) with parameters as previously described.[83,84] Result files from the search were used to generate input libraries for the spectral library in Spectronaut software (Version: 17.6.230428.55965, Quasar) following recommended default settings. A secondary spectral library was created directly from DDA data files using the Pulsar database search engine in Spectronaut. Combining results from both ProteinPilot-based and Pulsar-based DDA searches enhanced library comprehensiveness, incorporating newly identified peptides into existing proteins and adding newly detected proteins to the base library.

SWATH-MS data acquisition

The settings for SWATH-MS acquisition on the TripleTOF 6600 (SCIEX) and LC-MS instrument were specified as previously reported: a 100-variable window, a survey scan (MS1) from 350 to 1,250 m/z for 50 m, and high-sensitivity MS2 spectra from 100 to 1,500 m/z for 25 m. The total cycle time was approximately 2.5 s. Collision energy was applied to doubly charged precursors centered within the isolation window (1 m/z window overlap on the lower side of the window), using a collision energy equation like in DDA, with a collision energy spread of 5 eV.[83]

Data and statistical analysis

Comparative statistical analysis of protein identification and quantification was performed for the transfection conditions using Spectronaut software (Version: 17.0.221202.55965, Quasar) with our in-house spectral library for HEK293T. The standard Spectronaut settings, as outlined in the user manual, were utilized for this analysis. FDR threshold of 0.01 was required for protein identifications, and fold change cutoff of 1.5 ($p \leq 0.05$) required for differential protein expression. The process of the functional classifications was conducted as follows. The first step was to cluster protein expression data using two software programs, Cluster 3.0 and Java Treeview for hierarchical clustering and visualization of the results from proteome datasets. Clustered genes were decoded by Bulk Gene Searching Systems in Java (BGSSJ). BGSSJ is an XML-based Java application that systemizes lists of interesting genes and proteins for biological interpretation in the context of Gene Ontology.[85] Gene Ontology analysis was performed using R (v4.2.2) package WebGestalt Over-Representation Analysis (ORA), with a Benjamini-Hochberg test p value and FDR threshold of 0.05.[86]

DATA AND CODE AVAILABILITY

Raw data and MS processed files were deposited via ProteomeXchange to the PRIDE database, under project accession: PXD046574.

SUPPLEMENTAL INFORMATION

Supplemental information can be found online at https://doi.org/10.1016/j.omtm.2024.101278.

ACKNOWLEDGMENTS

The authors would like to thank the Bioprocessing Technology Institute and Biomedical Research Council of A*STAR (Agency for Science, Technology and Research), Singapore for the financial support for this research. Additionally, We express my heartfelt gratitude to Wang Loo Chien, Chee Fan Tan, and Mauro Galli for their valuable insights and thoughtful review of the manuscript. Their contributions have greatly improved the quality of this work. This work was supported by Bioprocessing Technology Institute and Biomedical Research Council of A*STAR (Agency for Science, Technology and Research), Singapore.

AUTHOR CONTRIBUTIONS

A.T.P. conducted proteomics studies, overall data analysis, prepared figures, and manuscript preparation. E.T. was involved in design of experiment (DoE) and conducted HEK293T cell culture, AAV titration experiments, and reviewed the manuscript. Y.J.K. reviewed the manuscript. S.K.N and X.B: Supervised the study, review and mentorship. All authors have read and approved the final manuscript.

DECLARATION OF INTERESTS

The authors declare no competing interests.

REFERENCES

1. Ail, D., Malki, H., Zin, E.A., and Dalkara, D. (2023). Adeno-Associated Virus (AAV) -Based Gene Therapies for Retinal Diseases: Where are We? Appl. Clin. Genet. *16*, 111–130. https://doi.org/10.2147/TACG.S383453.
2. Abulimiti, A., Lai, M.S.L., and Chang, R.C.C. (2021). Applications of adeno-associated virus vector-mediated gene delivery for neurodegenerative diseases and psychiatric diseases: Progress, advances, and challenges. Mech. Ageing Dev. *199*, 111549. https://doi.org/10.1016/j.mad.2021.111549.
3. Brown, N., Song, L., Kollu, N.R., and Hirsch, M.L. (2017). Adeno-Associated Virus Vectors and Stem Cells: Friends or Foes? Hum. Gene Ther. *28*, 450–463. https://doi.org/10.1089/hum.2017.038.
4. Bastola, P., Song, L., Gilger, B.C., and Hirsch, M.L. (2020). Adeno-Associated Virus Mediated Gene Therapy for Corneal Diseases. Pharmaceutics *12*, 767. https://doi.org/10.3390/pharmaceutics12080767.
5. Buning, H., Perabo, L., Coutelle, O., Quadt-Humme, S., and Hallek, M. (2008). Recent developments in adeno-associated virus vector technology. J. Gene Med. *10*, 717–733. https://doi.org/10.1002/jgm.1205.
6. Bera, A., and Sen, D. (2017). Promise of adeno-associated virus as a gene therapy vector for cardiovascular diseases. Heart Fail. Rev. *22*, 795–823. https://doi.org/10.1007/s10741-017-9622-7.
7. Berns, K.I., and Srivastava, A. (2019). Next Generation of Adeno-Associated Virus Vectors for Gene Therapy for Human Liver Diseases. Gastroenterol. Clin. North Am. *48*, 319–330. https://doi.org/10.1016/j.gtc.2019.02.005.
8. Brommel, C.M., Cooney, A.L., and Sinn, P.L. (2020). Adeno-Associated Virus-Based Gene Therapy for Lifelong Correction of Genetic Disease. Hum. Gene Ther. *31*, 985–995. https://doi.org/10.1089/hum.2020.138.
9. Pupo, A., Fernández, A., Low, S.H., François, A., Suárez-Amarán, L., and Samulski, R.J. (2022). AAV vectors: The Rubik's cube of human gene therapy. Mol. Ther. *30*, 3515–3541. https://doi.org/10.1016/j.ymthe.2022.09.015.
10. Fu, Q., Polanco, A., Lee, Y.S., and Yoon, S. (2023). Critical challenges and advances in recombinant adeno-associated virus (rAAV) biomanufacturing. Biotechnol. Bioeng. *120*, 2601–2621. https://doi.org/10.1002/bit.28412.
11. Joshi, P.R.H., Venereo-Sanchez, A., Chahal, P.S., and Kamen, A.A. (2021). Advancements in molecular design and bioprocessing of recombinant adeno-associated virus gene delivery vectors using the insect-cell baculovirus expression platform. Biotechnol. J. *16*, e2000021. https://doi.org/10.1002/biot.202000021.
12. Ou, J., Tang, Y., Xu, J., Tucci, J., Borys, M.C., and Khetan, A. (2024). Recent advances in upstream process development for production of recombinant adeno-associated virus. Biotechnol. Bioeng. *121*, 53–70. https://doi.org/10.1002/bit.28545.
13. Nguyen, T.N.T., Sha, S., Hong, M.S., Maloney, A.J., Barone, P.W., Neufeld, C., Wolfrum, J., Springs, S.L., Sinskey, A.J., and Braatz, R.D. (2021). Mechanistic model for production of recombinant adeno-associated virus via triple transfection of HEK293 cells. Mol. Ther. Methods Clin. Dev. *21*, 642–655. https://doi.org/10.1016/j.omtm.2021.04.006.
14. Li, J., Samulski, R.J., and Xiao, X. (1997). Role for highly regulated rep gene expression in adeno-associated virus vector production. J. Virol. *71*, 5236–5243. https://doi.org/10.1128/JVI.71.7.5236-5243.1997.
15. Xiao, X., Li, J., and Samulski, R.J. (1998). Production of high-titer recombinant adeno-associated virus vectors in the absence of helper adenovirus. J. Virol. *72*, 2224–2232. https://doi.org/10.1128/JVI.72.3.2224-2232.1998.
16. Chen, Y.H., Keiser, M.S., and Davidson, B.L. (2018). Adeno-Associated Virus Production, Purification, and Titering. Curr. Protoc. Mouse Biol. *8*, e56. https://doi.org/10.1002/cpmo.56.
17. Aponte-Ubillus, J.J., Barajas, D., Sterling, H., Aghajanirefah, A., Bardliving, C., Peltier, J., Shamlou, P., Roy, M., and Gold, D. (2020). Proteome profiling and vector yield optimization in a recombinant adeno-associated virus-producing yeast model. Microbiologyopen *9*, e1136. https://doi.org/10.1002/mbo3.1136.
18. Strasser, L., Boi, S., Guapo, F., Donohue, N., Barron, N., Rainbow-Fletcher, A., and Bones, J. (2021). Proteomic Landscape of Adeno-Associated Virus (AAV)-Producing HEK293 Cells. Int. J. Mol. Sci. *22*, 11499. https://doi.org/10.3390/ijms222111499.
19. Rosenberger, G., Koh, C.C., Guo, T., Röst, H.L., Kouvonen, P., Collins, B.C., Heusel, M., Liu, Y., Caron, E., Vichalkovski, A., et al. (2014). A repository of assays to quantify 10,000 human proteins by SWATH-MS. Sci. Data *1*, 140031. https://doi.org/10.1038/sdata.2014.31.

20. Liu, Y., Wang, M., Cheng, A., Yang, Q., Wu, Y., Jia, R., Liu, M., Zhu, D., Chen, S., Zhang, S., et al. (2020). The role of host eIF2α in viral infection. Virol. J. *17*, 112. https://doi.org/10.1186/s12985-020-01362-6.

21. Weinberg, M.S., Nicolson, S., Bhatt, A.P., McLendon, M., Li, C., and Samulski, R.J. (2014). Recombinant adeno-associated virus utilizes cell-specific infectious entry mechanisms. J. Virol. *88*, 12472–12484. https://doi.org/10.1128/JVI.01971-14.

22. Mattola, S., Aho, V., Bustamante-Jaramillo, L.F., Pizzioli, E., Kann, M., and Vihinen-Ranta, M. (2022). Nuclear entry and egress of parvoviruses. Mol. Microbiol. *118*, 295–308. https://doi.org/10.1111/mmi.14974.

23. Whittaker, G.R., and Helenius, A. (1998). Nuclear import and export of viruses and virus genomes. Virology *246*, 1–23. https://doi.org/10.1006/viro.1998.9165.

24. Guirimand, T., Delmotte, S., and Navratil, V. (2015). VirHostNet 2.0: surfing on the web of virus/host molecular interactions data. Nucleic Acids Res. *43*, D583–D587. https://doi.org/10.1093/nar/gku1121.

25. Chen, A.Y., and Qiu, J. (2010). Parvovirus infection-induced cell death and cell cycle arrest. Future Virol. *5*, 731–743. https://doi.org/10.2217/fvl.10.56.

26. Valerdi, K.M., Hage, A., van Tol, S., Rajsbaum, R., and Giraldo, M.I. (2021). The Role of the Host Ubiquitin System in Promoting Replication of Emergent Viruses. Viruses *13*, 369. https://doi.org/10.3390/v13030369.

27. Navratil, V., de Chassey, B., Meyniel, L., Delmotte, S., Gautier, C., André, P., Lotteau, V., and Rabourdin-Combe, C. (2009). VirHostNet: a knowledge base for the management and the analysis of proteome-wide virus-host interaction networks. Nucleic Acids Res. *37*, D661–D668. https://doi.org/10.1093/nar/gkn794.

28. Chung, C.H., Murphy, C.M., Wingate, V.P., Pavlicek, J.W., Nakashima, R., Wei, W., McCarty, D., Rabinowitz, J., and Barton, E. (2023). Production of rAAV by plasmid transfection induces antiviral and inflammatory responses in suspension HEK293 cells. Mol. Ther. Methods Clin. Dev. *28*, 272–283. https://doi.org/10.1016/j.omtm.2023.01.002.

29. Hemphill, D.D., McIlwraith, C.W., Slayden, R.A., Samulski, R.J., and Goodrich, L.R. (2016). Adeno-associated virus gene therapy vector scAAVIGF-I for transduction of equine articular chondrocytes and RNA-seq analysis. Osteoarthritis Cartilage *24*, 902–911. https://doi.org/10.1016/j.joca.2015.12.001.

30. Wallen, A.J., Barker, G.A., Fein, D.E., Jing, H., and Diamond, S.L. (2011). Enhancers of adeno-associated virus AAV2 transduction via high throughput siRNA screening. Mol. Ther. *19*, 1152–1160. https://doi.org/10.1038/mt.2011.4.

31. Barnes, C.R., Lee, H., Ojala, D.S., Lewis, K.K., Limsirichai, P., and Schaffer, D.V. (2021). Genome-wide activation screens to increase adeno-associated virus production. Mol. Ther. Nucleic Acids *26*, 94–103. https://doi.org/10.1016/j.omtn.2021.06.026.

32. Deyle, D.R., Hansen, R.S., Cornea, A.M., Li, L.B., Burt, A.A., Alexander, I.E., Sandstrom, R.S., Stamatoyannopoulos, J.A., Wei, C.L., and Russell, D.W. (2014). A genome-wide map of adeno-associated virus-mediated human gene targeting. Nat. Struct. Mol. Biol. *21*, 969–975. https://doi.org/10.1038/nsmb.2895.

33. Korbei, B. (2022). Ubiquitination of the ubiquitin-binding machinery: how early ESCRT components are controlled. Essays Biochem. *66*, 169–177. https://doi.org/10.1042/EBC20210042.

34. Wang, Y.E., Park, A., Lake, M., Pentecost, M., Torres, B., Yun, T.E., Wolf, M.C., Holbrook, M.R., Freiberg, A.N., and Lee, B. (2010). Ubiquitin-regulated nuclear-cytoplasmic trafficking of the Nipah virus matrix protein is important for viral budding. PLoS Pathog. *6*, e1001186. https://doi.org/10.1371/journal.ppat.1001186.

35. Nayak, R., and Pintel, D.J. (2007). Adeno-associated viruses can induce phosphorylation of eIF2alpha via PKR activation, which can be overcome by helper adenovirus type 5 virus-associated RNA. J. Virol. *81*, 11908–11916. https://doi.org/10.1128/JVI.01132-07.

36. Balakrishnan, B., Sen, D., Hareendran, S., Roshini, V., David, S., Srivastava, A., and Jayandharan, G.R. (2013). Activation of the cellular unfolded protein response by recombinant adeno-associated virus vectors. PLoS One *8*, e53845. https://doi.org/10.1371/journal.pone.0053845.

37. Whittaker, G.R., Kann, M., and Helenius, A. (2000). Viral entry into the nucleus. Annu. Rev. Cell Dev. Biol. *16*, 627–651. https://doi.org/10.1146/annurev.cellbio.16.1.627.

38. Nicolson, S.C., and Samulski, R.J. (2014). Recombinant adeno-associated virus utilizes host cell nuclear import machinery to enter the nucleus. J. Virol. *88*, 4132–4144. https://doi.org/10.1128/JVI.02660-13.

39. Hoad, M., Cross, E.M., Donnelly, C.M., Sarker, S., Roby, J.A., and Forwood, J.K. (2023). Structural Characterization of Porcine Adeno-Associated Virus Capsid Protein with Nuclear Trafficking Protein Importin Alpha Reveals a Bipartite Nuclear Localization Signal. Viruses *15*, 315. https://doi.org/10.3390/v15020315.

40. Hoad, M., Roby, J.A., and Forwood, J.K. (2021). Structural characterization of the porcine adeno-associated virus Po1 capsid protein binding to the nuclear trafficking protein importin alpha. FEBS Lett. *595*, 2793–2804. https://doi.org/10.1002/1873-3468.14209.

41. Snijder, E.J., Limpens, R.W.A.L., de Wilde, A.H., de Jong, A.W.M., Zevenhoven-Dobbe, J.C., Maier, H.J., Faas, F.F.G.A., Koster, A.J., and Bárcena, M. (2020). A unifying structural and functional model of the coronavirus replication organelle: Tracking down RNA synthesis. PLoS Biol. *18*, e3000715. https://doi.org/10.1371/journal.pbio.3000715.

42. Liu, Y.Y., Liang, X.D., Liu, C.C., Cheng, Y., Chen, H., Baloch, A.S., Zhang, J., Go, Y.Y., and Zhou, B. (2021). Fatty Acid Synthase Is Involved in Classical Swine Fever Virus Replication by Interaction with NS4B. J. Virol. *95*, e0078121. https://doi.org/10.1128/JVI.00781-21.

43. Osuna-Ramos, J.F., Reyes-Ruiz, J.M., and Del Ángel, R.M. (2018). The Role of Host Cholesterol During Flavivirus Infection. Front. Cell. Infect. Microbiol. *8*, 388. https://doi.org/10.3389/fcimb.2018.00388.

44. Basner-Tschakarjan, E., and Mingozzi, F. (2014). Cell-Mediated Immunity to AAV Vectors, Evolving Concepts and Potential Solutions. Front. Immunol. *5*, 350. https://doi.org/10.3389/fimmu.2014.00350.

45. Muhuri, M., Maeda, Y., Ma, H., Ram, S., Fitzgerald, K.A., Tai, P.W., and Gao, G. (2021). Overcoming innate immune barriers that impede AAV gene therapy vectors. J. Clin. Invest. *131*, e143780. https://doi.org/10.1172/JCI143780.

46. Shayakhmetov, D.M. (2010). Virus infection recognition and early innate responses to non-enveloped viral vectors. Viruses *2*, 244–261. https://doi.org/10.3390/v2010244.

47. Wang, Y., Fu, Q., Lee, Y.S., Sha, S., and Yoon, S. (2023). Transcriptomic features reveal molecular signatures associated with recombinant adeno-associated virus production in HEK293 cells. Biotechnol. Prog. *39*, e3346. https://doi.org/10.1002/btpr.3346.

48. Calcedo, R., Chichester, J.A., and Wilson, J.M. (2018). Assessment of Humoral, Innate, and T-Cell Immune Responses to Adeno-Associated Virus Vectors. Hum. Gene Ther. Methods *29*, 86–95. https://doi.org/10.1089/hgtb.2018.038.

49. Dauletbekov, D.L., Pfromm, J.K., Fritz, A.K., and Fischer, M.D. (2019). Innate Immune Response Following AAV Administration. Adv. Exp. Med. Biol. *1185*, 165–168. https://doi.org/10.1007/978-3-030-27378-1_27.

50. Hamilton, B.A., and Wright, J.F. (2021). Challenges Posed by Immune Responses to AAV Vectors: Addressing Root Causes. Front. Immunol. *12*, 675897. https://doi.org/10.3389/fimmu.2021.675897.

51. Hareendran, S., Balakrishnan, B., Sen, D., Kumar, S., Srivastava, A., and Jayandharan, G.R. (2013). Adeno-associated virus (AAV) vectors in gene therapy: immune challenges and strategies to circumvent them. Rev. Med. Virol. *23*, 399–413. https://doi.org/10.1002/rmv.1762.

52. Timpe, J.M., Verrill, K.C., Black, B.N., Ding, H.F., and Trempe, J.P. (2007). Adeno-associated virus induces apoptosis during coinfection with adenovirus. Virology *358*, 391–401. https://doi.org/10.1016/j.virol.2006.08.042.

53. Aslanidi, G., Lamb, K., and Zolotukhin, S. (2009). An inducible system for highly efficient production of recombinant adeno-associated virus (rAAV) vectors in insect Sf9 cells. Proc. Natl. Acad. Sci. USA *106*, 5059–5064. https://doi.org/10.1073/pnas.0810614106.

54. Gallo-Ramirez, L.E., Ramirez, O.T., and Palomares, L.A. (2011). Intracellular localization of adeno-associated viral proteins expressed in insect cells. Biotechnol. Prog. *27*, 483–493. https://doi.org/10.1002/btpr.565.

55. Herrmann, A.K., Große, S., Börner, K., Krämer, C., Wiedtke, E., Gunkel, M., and Grimm, D. (2019). Impact of the Assembly-Activating Protein on Molecular Evolution of Synthetic Adeno-Associated Virus Capsids. Hum. Gene Ther. *30*, 21–35. https://doi.org/10.1089/hum.2018.085.

56. Ruffing, M., Zentgraf, H., and Kleinschmidt, J.A. (1992). Assembly of viruslike particles by recombinant structural proteins of adeno-associated virus type 2 in insect cells. J. Virol. *66*, 6922–6930. https://doi.org/10.1128/JVI.66.12.6922-6930.1992.

57. Calistri, A., Reale, A., Palù, G., and Parolin, C. (2021). Why Cells and Viruses Cannot Survive without an ESCRT. Cells *10*, 483.

58. Miller, S., and Krijnse-Locker, J. (2008). Modification of intracellular membrane structures for virus replication. Nat. Rev. Microbiol. *6*, 363–374. https://doi.org/10.1038/nrmicro1890.

59. Spuul, P., Balistreri, G., Hellström, K., Golubtsov, A.V., Jokitalo, E., and Ahola, T. (2011). Assembly of alphavirus replication complexes from RNA and protein components in a novel trans-replication system in mammalian cells. J. Virol. *85*, 4739–4751. https://doi.org/10.1128/JVI.00085-11.

60. Barajas, D., Kovalev, N., Qin, J., and Nagy, P.D. (2015). Novel mechanism of regulation of tomato bushy stunt virus replication by cellular WW-domain proteins. J. Virol. *89*, 2064–2079. https://doi.org/10.1128/JVI.02719-14.

61. Campsteijn, C., Vietri, M., and Stenmark, H. (2016). Novel ESCRT functions in cell biology: spiraling out of control? Curr. Opin. Cell Biol. *41*, 1–8. https://doi.org/10.1016/j.ceb.2016.03.008.

62. Hurley, J.H. (2015). ESCRTs are everywhere. EMBO J. *34*, 2398–2407. https://doi.org/10.15252/embj.201592484.

63. Jiang, B., Himmelsbach, K., Ren, H., Boller, K., and Hildt, E. (2015). Subviral Hepatitis B Virus Filaments, like Infectious Viral Particles, Are Released via Multivesicular Bodies. J. Virol. *90*, 3330–3341. https://doi.org/10.1128/JVI.03109-15.

64. Shields, S.B., and Piper, R.C. (2011). How ubiquitin functions with ESCRTs. Traffic *12*, 1306–1317. https://doi.org/10.1111/j.1600-0854.2011.01242.x.

65. Bleker, S., Pawlita, M., and Kleinschmidt, J.A. (2006). Impact of capsid conformation and Rep-capsid interactions on adeno-associated virus type 2 genome packaging. J. Virol. *80*, 810–820. https://doi.org/10.1128/JVI.80.2.810-820.2006.

66. Ding, W., Zhang, L., Yan, Z., and Engelhardt, J.F. (2005). Intracellular trafficking of adeno-associated viral vectors. Gene Ther. *12*, 873–880. https://doi.org/10.1038/sj.gt.3302527.

67. Ding, W., Zhang, L.N., Yeaman, C., and Engelhardt, J.F. (2006). rAAV2 traffics through both the late and the recycling endosomes in a dose-dependent fashion. Mol. Ther. *13*, 671–682. https://doi.org/10.1016/j.ymthe.2005.12.002.

68. Herrmann, A.K., and Grimm, D. (2018). High-Throughput Dissection of AAV-Host Interactions: The Fast and the Curious. J. Mol. Biol. *430*, 2626–2640. https://doi.org/10.1016/j.jmb.2018.05.022.

69. Robinson, M., Schor, S., Barouch-Bentov, R., and Einav, S. (2018). Viral journeys on the intracellular highways. Cell. Mol. Life Sci. *75*, 3693–3714. https://doi.org/10.1007/s00018-018-2882-0.

70. Isono, E. (2021). ESCRT Is a Great Sealer: Non-Endosomal Function of the ESCRT Machinery in Membrane Repair and Autophagy. Plant Cell Physiol. *62*, 766–774. https://doi.org/10.1093/pcp/pcab045.

71. Agromayor, M., Carlton, J.G., Phelan, J.P., Matthews, D.R., Carlin, L.M., Ameer-Beg, S., Bowers, K., and Martin-Serrano, J. (2009). Essential role of hIST1 in cytokinesis. Mol. Biol. Cell *20*, 1374–1387. https://doi.org/10.1091/mbc.e08-05-0474.

72. Ariumi, Y., Kuroki, M., Maki, M., Ikeda, M., Dansako, H., Wakita, T., and Kato, N. (2011). The ESCRT system is required for hepatitis C virus production. PLoS One *6*, e14517. https://doi.org/10.1371/journal.pone.0014517.

73. Chen, B.J., and Lamb, R.A. (2008). Mechanisms for enveloped virus budding: can some viruses do without an ESCRT? Virology *372*, 221–232. https://doi.org/10.1016/j.virol.2007.11.008.

74. Wegner, C.S., Rodahl, L.M.W., and Stenmark, H. (2011). ESCRT proteins and cell signalling. Traffic *12*, 1291–1297. https://doi.org/10.1111/j.1600-0854.2011.01210.x.

75. Corless, L., Crump, C.M., Griffin, S.D.C., and Harris, M. (2010). Vps4 and the ESCRT-III complex are required for the release of infectious hepatitis C virus particles. J. Gen. Virol. *91*, 362–372. https://doi.org/10.1099/vir.0.017285-0.

76. Han, H., and Hill, C.P. (2019). Structure and mechanism of the ESCRT pathway AAA+ ATPase Vps4. Biochem. Soc. Trans. *47*, 37–45. https://doi.org/10.1042/BST20180260.

77. Li, C., He, Y., Nicolson, S., Hirsch, M., Weinberg, M.S., Zhang, P., Kafri, T., and Samulski, R.J. (2013). Adeno-associated virus capsid antigen presentation is dependent on endosomal escape. J. Clin. Invest. *123*, 1390–1401. https://doi.org/10.1172/JCI66611.

78. Penzes, J.J., Chipman, P., Bhattacharya, N., Zeher, A., Huang, R., McKenna, R., and Agbandje-McKenna, M. (2021). Adeno-associated Virus 9 Structural Rearrangements Induced by Endosomal Trafficking pH and Glycan Attachment. J. Virol. *95*, e0084321. https://doi.org/10.1128/JVI.00843-21.

79. Kanna, M., Nakatsu, Y., Yamamotoya, T., Encinas, J., Ito, H., Okabe, T., Asano, T., and Sakaguchi, T. (2022). Roles of peptidyl prolyl isomerase Pin1 in viral propagation. Front. Cell Dev. Biol. *10*, 1005325. https://doi.org/10.3389/fcell.2022.1005325.

80. Ding, Z., Bae, Y.H., and Roy, P. (2012). Molecular insights on context-specific role of profilin-1 in cell migration. Cell Adh. Migr. *6*, 442–449. https://doi.org/10.4161/cam.21832.

81. Grieger, J.C., Soltys, S.M., and Samulski, R.J. (2016). Production of Recombinant Adeno-associated Virus Vectors Using Suspension HEK293 Cells and Continuous Harvest of Vector From the Culture Media for GMP FIX and FLT1 Clinical Vector. Mol. Ther. *24*, 287–297. https://doi.org/10.1038/mt.2015.187.

82. Aurnhammer, C., Haase, M., Muether, N., Hausl, M., Rauschhuber, C., Huber, I., Nitschko, H., Busch, U., Sing, A., Ehrhardt, A., and Baiker, A. (2012). Universal real-time PCR for the detection and quantification of adeno-associated virus serotype 2-derived inverted terminal repeat sequences. Hum. Gene Ther. Methods *23*, 18–28. https://doi.org/10.1089/hgtb.2011.034.

83. Sim, K.H., Liu, L.C.Y., Tan, H.T., Tan, K., Ng, D., Zhang, W., Yang, Y., Tate, S., and Bi, X. (2020). A comprehensive CHO SWATH-MS spectral library for robust quantitative profiling of 10,000 proteins. Sci. Data *7*, 263. https://doi.org/10.1038/s41597-020-00594-z.

84. Schubert, O.T., Gillet, L.C., Collins, B.C., Navarro, P., Rosenberger, G., Wolski, W.E., Lam, H., Amodei, D., Mallick, P., MacLean, B., and Aebersold, R. (2015). Building high-quality assay libraries for targeted analysis of SWATH MS data. Nat. Protoc. *10*, 426–441. https://doi.org/10.1038/nprot.2015.015.

85. Juan, H.F., and Huang, H.C. (2007). Bioinformatics: microarray data clustering and functional classification. Methods Mol. Biol. *382*, 405–416. https://doi.org/10.1007/978-1-59745-304-2_25.

86. Liao, Y., Wang, J., Jaehnig, E.J., Shi, Z., and Zhang, B. (2019). WebGestalt 2019: gene set analysis toolkit with revamped UIs and APIs. Nucleic Acids Res. *47*, W199–W205. https://doi.org/10.1093/nar/gkz401.